THE SENSITIVITY OF Hα PROFILES TO RAPID ELECTRON BEAM FLUCTUATIONS*

Richard C. Canfield and Kenneth G. Gayley

Center for Astrophysics and Space Sciences and Department of Physics
University of California
San Diego, California

ABSTRACT

In order to understand the temporal relationship between Hα and hard X-ray emission predicted by the nonthermal electron thick target model of impulsive-phase energy transport we have computed time-dependent theoretical Hα profiles for the dynamic model atmospheres of Fisher, Canfield and McClymont (1985b), which simulate the effects of an impulsively initiated power-law beam of electrons.

On the basis of our physical analysis we expect a very rapid Hα response to an instantaneous increase in the flux of a nonthermal deka-keV electron beam, as compared to the timescale associated with the propagation of these electrons over characteristic flare coronal loop spatial scales. The amplitude and timescale of this response vary over the Hα profile, and show effects which arise from three different physical mechanisms. First, there is an impulsive initial rise, on the chromospheric heating timescale, which has greatest amplitude at line center. Second, there is a slower component, on hydrogen thermal ionization timescales, which is most apparent in the blue wing, Third, there is a delayed response, associated with the formation of the chromospheric condensation, which is most apparent in the red wing. This latter component dominates over ionization effects on the red side of Hα and, to a lesser extent, at line center.

We conclude that observational efforts to test the thick target nonthermal electron model through detection of impulsive Hα brightenings associated with impulsive hard X-ray or microwave bursts should initially focus attention on Hα line center. Additional simultaneous blue-wing measurements will have substantial diagnostic potential. However, red wing measurements are potentially deceptive, since the prompt enhancements on the chromospheric heating timescale are much smaller than the ~1 s delayed enhancements due to chromospheric condensations, which are not uniquely associated with either nonthermal electron beams or conduction fronts.

INTRODUCTION

Study of the morphology and timing of Hα emission, relative to hard X-ray and microwave emission, during the impulsive phase provides a useful test through which one can discriminate between alternate models for impulsive phase energy transport. For example, are deka-keV electrons the dominant mechanism of energy transport from the hot flare corona (Lin and Hudson, 1976), or are lower

* Supported by the National Aeronautics and Space Administration, under grant NSG-7406, and by the National Science Foundation, under grant ATM84-15793.

energy electrons in a nonclassical conduction front (Brown, Melrose, and Spicer 1979) more important? In the former case, one expects synchronism between Hα and microwaves or hard X-rays on timescales much less than 1 s, whereas in the latter delays of several seconds are to be expected between the hard X-ray or microwave event and its primary Hα counterpart.

Temporal resolution of order 1 s is required to discriminate between conduction-front and energetic-particle energy tranport models. It is also necessary to have spatial resolution, since not all parts of the flare necessarily reflect the same transport process. In the past the lack of adequate temporal resolution led to much confusion about time delays between hard X-rays (or microwaves) and Hα (cf. Vorpahl 1972 and Zirin 1978). However, the development of two-dimensional digital detector systems enabled the first observations with sufficient temporal resolution, which have been obtained recently by Kaempfer and Schoechlin (1982) and Kaempfer and Magun (1983). In a study of one flare with 1.4 s and 100 ms temporal resolution in Hα and microwaves respectively, Kaempfer and Magun found evidence for both fast electron transport, at one site of a flare, and hydrodynamic or nonclassical conductive transport, at other sites of the same flare. At the former site they observed Hα and microwave synchronism within two seconds; the lack of delays at different microwave frequencies also supported an energetic electron interpretation. At the latter sites, delays of about 10 s were observed. The authors showed that these delays are consistent with the propagation of disturbances at about 2000 km/s, i.e. roughly the same velocities expected for collisionless conduction fronts.

In this paper we address a specific technical question: for such simultaneous observations with microwaves or hard X-rays, what is the most appropriate point within the Hα line profile? The observations by Kaempfer and Schoechlin (1982) and Kaempfer and Magun (1983) were made with a narrow-band filter centered on the Hα line. Other observations are currently in progress elsewhere, some of which use a filter centered on the line, while others use the red wing. Which of these positions within the Hα line profile is the best test of energy tranport mechanisms? Which of these positions, or combinations of positions, offers the most valuable diagnostic potential? To answer these questions, our approach is not to try to simulate all the complexity found in real flares; we know from hard X-ray data that, for example, that there is no compelling evidence for preferred values of beam durations or intensities. Instead we discuss in this paper a highly idealized computer simulation which leads to an understanding that can be used to both guide and interpret simultaneous observations in Hα and microwaves or hard X-rays.

COMPUTATIONS

In this paper we compute theoretical time-dependent Hα line profiles for selected times in the sequence of model atmospheres of Fisher, Canfield and McClymont (1985b), henceforth FCM. These models simulate the dynamic response of a loop atmosphere to Coulomb heating by a power-law beam of nonthermal electrons injected at the coronal loop apex. FCM assumed that an electron beam was turned on instantaneously, at a specified value of F_{20} (the equivalent flux of nonthermal electrons above a 20 keV energy cutoff) and then turned off after 5 s. To study the response of Hα on short timescales, we focus our attention on the first few seconds.

The method used for the computation of the time dependent Hα profiles in this paper is an extension of the previous static calculations of Canfield, Gunkler and Ricchiazzi (1984), henceforth CGR. For the model atmospheres at certain instants, available from FCM, we solve the probabilistic radiative transfer equation (Canfield, McClymont, and Puetter 1984) for a 4-level-plus-continuum hydrogen atom. Complete redistribution within a pure Doppler absorption coefficient profile is adopted for the Lyman lines (following Milkey and Mihalas 1973). The absorption coefficient profile for all subordinate transitions has a Doppler core and wings due to both the linear Stark effect (we assume a Holtsmark profile) and resonance broadening (hydrogen-hydrogen collisions; see Mihalas 1978). Our use of probabilistic radiative transfer in the computations of Hα line profiles is consistent with its use by FCM in the energy equation, and its physical limitations are discussed in detail in FCM and CGR. The major limitations on accuracy of radiative transfer aspects of our calculation probably accrue both from the use of probabilistic methods and from the assumption of Doppler core redistribution for the Lyman lines. We estimate that the Hα profiles computed here are limited in their quantitative accuracy to about a factor of two, as a result of these two factors.

The sole difference between the methods used here and those used by CGR lies in the treatment of velocity fields and radiative transfer in the equations describing the level populations of the model hydrogen atom. In the present calcuation the fractional population ϕ_i of the quantum state i of hydrogen is determined by the rate equation

$$\dot{\phi}_i \equiv \partial\phi_i/\partial t = \sum_{j\neq i} \left[R_{ji}\phi_j - R_{ij}\phi_i\right] \tag{1}$$

and the radiative and collisional transition rate coefficients R_{ij} between states i and h, subject to the constraints that

$$\dot{\phi}_2 = \dot{\phi}_3 = \dot{\phi}_4 = 0 \tag{2a}$$

$$\dot{\phi}_1 = -\dot{\phi}_C \tag{2b}$$

and

$$\dot{\phi}_C = \dot{\phi}_C^{(2)}, \tag{2c}$$

where $\dot{\phi}_C^{(2)}$ is the value computed for a 2-level-plus-continuum hydrogen atom by FCM. These constraints given allow us to use the FCM results, rather than having to replace them by a simulation that includes, from the beginning, a full 4-level-plus-continuum hydrogen atom. The use of the more complete model of the hydrogen atom would have only minor effects on the ionization state and energy loss rate as a function of time, yet would impose stringent computational demands. There is no reason to doubt the validity, on the factor of two level that characterizes the calculations throughout, of the approximations made in imposing these constraints, because the rates among the bound levels are so much faster than the rates from bound levels to the continuum; for completeness, we will return to a quantitative discussion of the self-consistency of this assumption below. Our solution to the combined set of radiative transfer and atomic population equations (2) for any FCM model atmosphere at any chosen time gives a self-consistent set of radiation fields and source functions for all transitions within the 4-level-plus-continuum hydrogen atom, including Hα. From

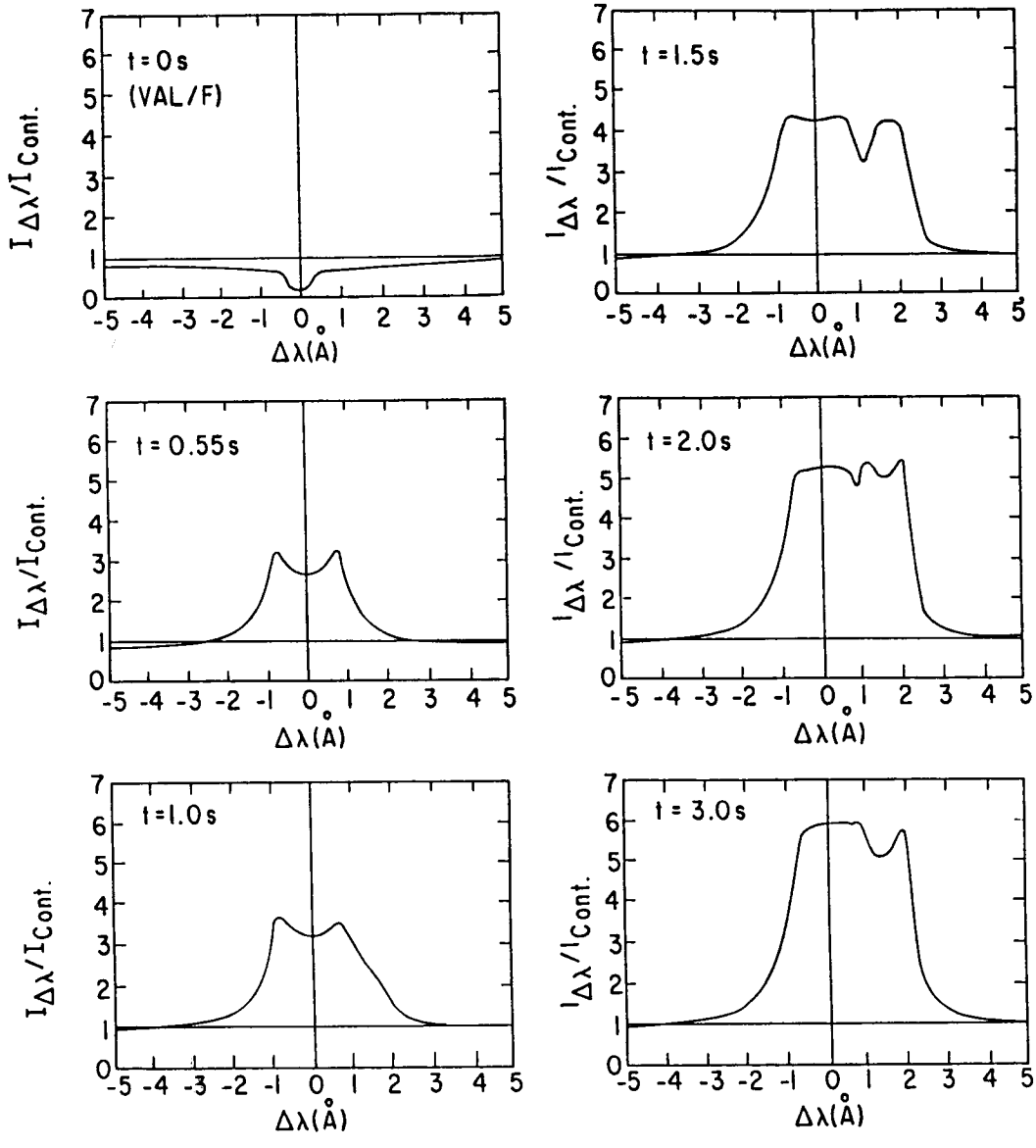

Fig. 1. - Theoretical Hα line profiles for the electron beam heated model atmospheres of Fisher, Canfield and McClymont (1985b), at the indicated times relative to the instantaneous start of flare heating.

this solution, and the columnar dependence of density, hydrogen ionized fraction, and velocity from the FCM models, we know all quantities required to compute the Hα line profiles.

Figure 1 shows Hα profiles at 6 selected times of interest from the FCM $F_{20} = 10^{11}$ ergs cm^{-2} s^{-1} simulation; the electron beam heating in the FCM simulation was turned on instantaneously at t = 0 and remained constant for the entire period shown in the figure. It is clear that at t = 0.55 s the Hα-emitting chromosphere is enhanced considerably; its behavior on timescales shorter than 0.55 s is discussed below. The profile at 0.55 s is still symmetric; the Hα-emitting chromosphere is not yet moving. By t = 1.0 s an enhanced red wing is formed, which is the first indication of chromospheric mass motions. By t = 1.5 s one sees that there are two components of the Hα line profile, one shifted and one not. The further evolution of these two components can be seen in the subsequent panels at t = 2.0 and 3.0 s. The unshifted component is broad and is initially centrally reversed; it fills in as time passes. This tendency for the reversal to fill in is primarily a consequence of the shifting of the region of formation to a more dense region of the chromosphere, as the region of formation of unshifted Hα emission rapidly shifts to greater column depths. It is secondarily due to seeing even further into the chromosphere at line center due to Doppler shifting of overlying reversing material in the condensation. The shifted component is unreversed initially, while it is optically thin, but a central reversal appears as the moving material becomes optically thick. The moving material is the chromospheric condensation, shown by FCM to be a thin slab of chromospheric material rapidly cooled by the enhanced radiative loss rate associated with compression of this region driven by explosive chromospheric evaporation of adjacent overlying material. The redshift of the emission from the condensation decreases perceptibly between 1.5 and 3 s, as a consequence of its rapid slowing.

We note that the computed Hα profiles are much brighter than typical observed line profiles. The profiles show that this emission comes from both the moving condensation and the essentially static underlying chromosphere, both of which exhibit high pressure. CGR showed that high pressure static atmospheres produce very bright Hα profiles when the conductive flux is not large enough to evaporate much of the flare chromosphere. It is premature, however, to compare these theoretical profiles to observations. As shown by Canfield and Ricchiazzi (1980), the probabilistic radiative transfer methods upon which both the FCM model atmospheres and our Hα profiles are based are only accurate to the factor of two level for static atmospheres such as the VAL/F (Vernazza, Avrett, and Loeser 1981). For dynamic atmospheres in which velocity gradients exceed well-understood limits additional systematic errors arise due to the use of the probabilistic methods. It is known that these limits are exceeded in the FCM atmospheres, in the vicinity of the condensation front. Hence it is important to recognize that while the Hα profiles of Figure 1 are qualitatively well founded, and are based on a method that correctly describes the dominant physical processes associated with photon escape in static atmospheres, one should not attribute significance to the intensity, relative to the background continuum, on the factor of two level.

In Figure 2 we contrast the time dependence of the relative intensity of various parts of the Hα line profile. Bearing in mind that the intensity scale used in the upper panel of Figure 2 is much different from that used in the center and lower panels, it is clear that there is considerable difference, in

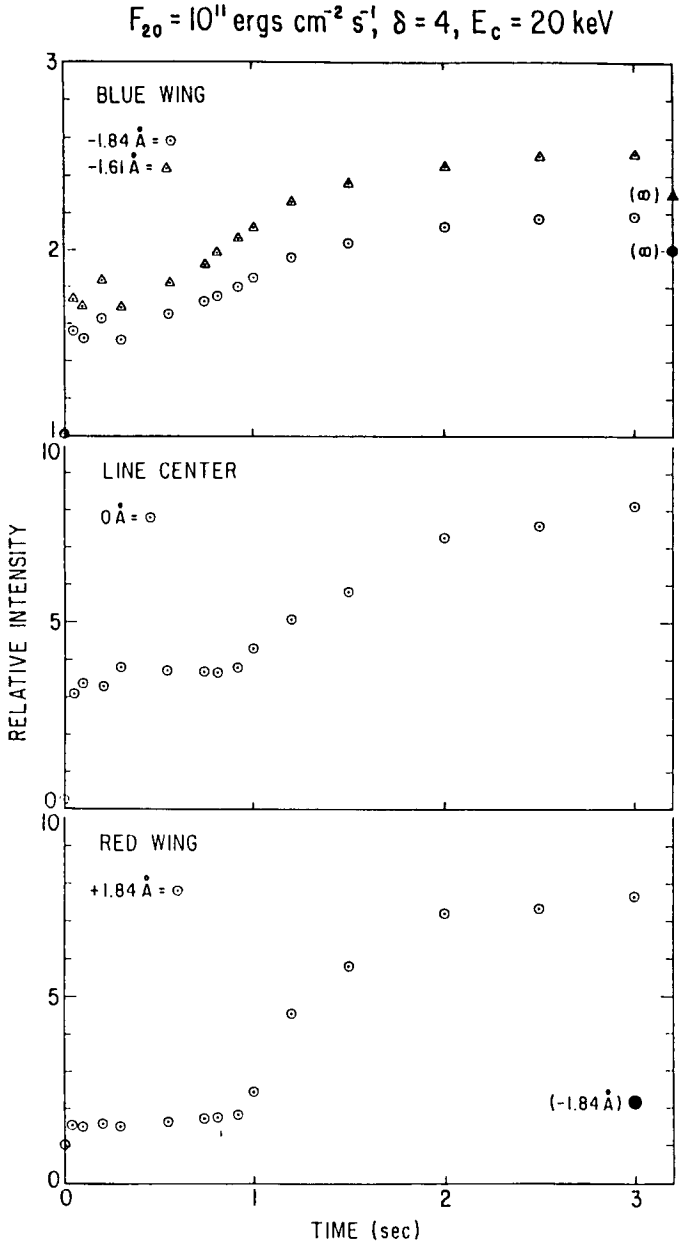

Fig. 2. - The relative intensity of the Hα line profile at the indicated spectral positions, for electron-beam-heated dynamic model atmospheres of Fisher, Canfield and McClymont (1985b), as a function of time relative to the moment of instantaneous initiation of flare heating. The filled symbols marked (∞) in the upper panel are from the hydrostatic calculation of Canfield, Gunkler and Ricchiazzi (1984). The filled symbol in the lower panel is our blue wing result at t = 3 s.

both amplitude and functional form, of the time dependence between the blue wing, the line center, and the red wing. Each point in Figure 2 corresponds to one of a limited number of times at which a dynamic model atmosphere from the FCM simulation is available. Between the first and second points (at t = 0 and 0.05 s respectively) the intensity jumps on a timescale not resolved in the figure, but temporally and spatially resolved in the computations themselves. The relative increase of this initial jump is much greater at line center than in either wing. In the blue wing, at both -1.61 and -1.84 Å, there is also a slower increase, on a timescale ~0.3 - 0.4 s; our analysis suggests that this is an ionization effect. Finally, at both line center and in the red wing, one sees a delayed increase (starting at about 1 s), which is due to the formation of the chromospheric condensation. We now turn to a discussion of the physical origins of these effects.

ANALYSIS

The three timescales on which the Hα line profile varies in our numerical simulation can understood in terms of the timescales for electron beam heating, thermal ionization, and chromospheric condensation.

ELECTRON BEAM HEATING

In the first approximation, the flare chromosphere reaches a quasi-equilibrium on the longer of two timescales, those for heating

$$t_h = E_{th}/Q_b \tag{3}$$

and radiative cooling

$$t_r = E_{th}/R. \tag{4}$$

The duration of this quasi-equilibrium is limited to values much less than the hydrodynamic timescale

$$t_p = H/c_s. \tag{5}$$

Here E_{th} is the specific (per hydrogen nucleus) mean thermal energy $\frac{3}{2}kT(1+x)$, T is the electron and ion temperature, k is Boltzmann's constant, x is the hydrogen ionized fraction, Q_b is the specific electron beam heating rate, R is the specific radiative cooling rate, H is the local density scale height for hydrogen nuclei, and c_s is the sound speed. The value of t_p is of order 5 - 10 s in the flare chromosphere. For the impulsive phenomena that interest us here we need consider only t_h and t_r.

In this study we are interested primarily in the region of the atmosphere from which the flare Hα emission originates. Table 1 identifies physical parameters of interest in this region: N is the column depth of maximum contribution to the Hα emission at the specified spectral location within the line profile and x and T are the hydrogen ionized fraction and temperature at this depth. We focus our attention on the depths of maximum contribution at two times: 1) t = 0 s, before any shift of the emitting region into the deeper chromosphere has started, and 2) at t ~ 1.5 s, after the emitting region has

shifted into the deeper chromosphere and the condensation has been formed. Table 2 shows that if $F_{20} = 10^{11}$ ergs cm^{-2} s^{-1}, the heating timescale t_h is very short at the depths that are of interest when the beam is first turned on--less than 10 ms. Because the radiation timescale t_r is so long, and the t_h is so much less than the pressure equilibration timescale t_p, it is clear that either the temperature or the hydrogen ionized fraction is going to increase very rapidly. Since both the rate and amount of energy that can go into ionization is limited, while the rate and amount that can go into thermal form is much more weakly constrained, the temperature of the beam-heated chromosphere will increase on timescales less than 10 ms, if the beam energy flux $F_{20} = 10^{11}$ ergs cm^{-2} s^{-1}. At t = 1.5 s the heating timescale is longer, especially in the wings of Hα, but is still about an order of magnitude less than the electron transit timescale $t_e = L/v_e$, where L is the characteristic length of a flare loop and v_e is the characteristic velocity of a nonthermal electron, if $L = 10^4$ km and E_e = 100 keV. A range of values is given for the red wing at t = 1.5 s because this emission is distributed rather evenly over the condensation and the upper uncondensed material.

TABLE 1. - PHYSICAL PARAMETERS IN THE Hα CHROMOSPHERE AT DEPTHS OF MAXIMUM CONTRIBUTION TO Hα EMISSION

t = 0 s	N(cm^{-2})	T(K)	x
Blue Wing (-1.8 Å)	1.5×10^{20}	6700	0.05
Line Center	6.2×10^{18}	7600	0.50
Red Wing (+1.8 Å)	1.5×10^{20}	6700	0.05
t = 1.5 s	**N(cm^{-2})**	**T(K)**	**x**
Blue Wing (-1.8 Å)	3.6×10^{20}	11,800	0.95
Line Center	6.0×10^{19}	59,000	1.00
Red Wing (+1.8 Å)†	3.6×10^{20}	11,800	0.95
	2.7×10^{19}	22,400	1.00

† Red wing emission originates in both the condensation and the uncompressed upper chromosphere.

TABLE 2. - TIMESCALES (SECONDS) IN THE Hα CHROMOSPHERE $F_{20} = 10^{11}$ ergs cm^{-2} s^{-1}

	t = 0 s		t = 1.5 s	
Wavelength ($\Delta\lambda$)	heating	radiation	heating	radiation
Blue Wing (-1.8 Å)	7×10^{-3}	$1 \times 10^{+2}$	2×10^{-1}	2×10^{-1}
Line Center	2×10^{-3}	$6 \times 10^{+0}$	2×10^{-2}	2×10^{-2}
Red Wing (+1.8 Å)	7×10^{-3}	$1 \times 10^{+2}$	$1 \times 10^{-1-2}$	$1 \times 10^{-1-2}$

Several comments are in order. It is apparent that the sudden jump in the Hα intensity at all three Δλ values in Figure 2 in the interval $0 < t < .05$ s is a consequence of the short heating timescale in the region of initial formation of Hα. Hence, except for other complications (see below), it appears that all three spectral positions within Hα would be useful for high-intensity electron beam timing experiments, since all heating timescales are much less than beam transit timescales. Even though the heating timescale is 1 - 2 orders of magnitude longer after the beam is established, it still remains about one order less than t_e. Third, the table confirms the quasi-equilibrium interpretation of the slowly-rising plateau seen at line center and the red wing during the first second of Figure 2; to the precision given in Table 2, $t_h = t_r$. One should therefore expect Hα to track beam temporal variations, at high electron beam flux levels, down to timescales well under 1 s. Finally, it is hardly surprising that substantial Hα emission is generated in the flare chromosphere, given the large temperatures at the depths of maximum contribution given in Table 1. The hydrogen ionized fraction is much higher in the Hα flare chromosphere than in the preflare, but no so high that the chromosphere is optically thin at line center.

THERMAL IONIZATION

The gradual increase in the blue wing emission evident in Figure 2 on a timescale of about 0.3 - 0.4 seconds suggests a slow drift toward an equilibrium that must be only quasi-steady on a grander timescale as macroscopic effects such as pressure equilibration set in. What physical effect controls the timescale of this approach to equilibrium, or more accurately, what is the slowest of the many physical effects present? The temperature and density of the emitting region are important to the total emission, but the temperature equilibrates rapidly, as described above. Also, the density changes only on the much longer hydrodynamic timescale. Is then the relevant timescale that for the atomic level populations to equilibrate? The bound-bound rate coefficients in equation (1) are so large that the level populations equilibrate with each other extremely rapidly, but the continuum rates are much slower and so the continuum equilibration takes much longer. Thus the ionization timescale is a likely candidate for the slow-paced driving timescale in this equilibration process.

The ionization timescale manifests itself in a gradual increase in the optically thin component of the wing emission. This is due to the effects of Stark broadening of the Hα absorption coefficient profile caused by interactions of hydrogen atoms with free electrons. As ionization progresses and the free electron density increases, the broadened profiles produce an enhancement of the wing emission from the ionizing region. (This emission is optically thin, so is superimposed on top of the fairly constant optically thick wing emission from the photosphere, but it contributes strongly to the total wing emission.) Thus we expect a close correlation between the local ionization timescale and the timescale for increase of the local contribution to the total wing emission. This assumption can be tested by focusing on the region where emission in the wings (e.g. at $\Delta\lambda = -1.8$ and -1.6 Å) is most important, and calculating the ionization timescales directly from the local rate

equations (1).

There are two ways in which the local populations effect the local contribution to the Hα wing emission. First, the absorption coefficient profile may become wider due to larger free electron density and associated increased Stark broadening, as mentioned above. Second, the population of the second level of hydrogen may increase, increasing the Hα opacity (recall that the emission being considered is optically thin). This second effect is highly dependent on the rate coefficient primarily responsible for populating level 2, which is the $1 \rightarrow 2$ radiative rate, and as such is proportional to the local Lα radiation field, whose origins are highly nonlocal. If these nonlocal effects dominated the local wing rise, it would be impossible to analyze the timescale in terms of local equilibration timescales such as the ionization timescale. Fortunately, our results indicate that the dominant effect is the absorption coefficient profile, not the second level opacity. Hence the ionization timescales are the most relevant to the wing rise, and these can be found at least approximately by considering only the local conditions, i.e., the local rate coefficients.

Finding a simple approximation to these ionization timescales based on the local conditions is complicated by the fact that the rate equations (1) are nonlinear, owing to the dependence of the collisional and radiative recombination rate coefficients on the electron density and thus on the continuum population itself. But the local behavior of these equations can be approximated by linearizing about a given point taken from the simulations. The problem then reduces to the solution of a linear system of first order differential equations, whose eigenvalues are thus the equilibration rates of the various normal modes of decay to equilibrium. The smallest of these eigenvalues will correspond to the most slowly decaying mode, and will therefore give the overall net equilibration rate. Of course, this can only approximate the true equilibration rate because the equilibrium approached by the linearized system will deviate from the true equilibrium. This probably introduces an uncertainty of a factor of two or so in the rate predicted by this simple analysis.

Linearization of the rate coefficients with respect to their dependence on the continuum population is accomplished by writing the vector ϕ of atomic level populations (ϕ_1, ... ϕ_4, ϕ_C in our case) as $\phi = \phi_0 + \delta\phi$, where ϕ_0 is the locally determined equilibrium population vector. The linearized form of equation (1) is then

$$\delta\dot{\phi} = R\,\phi_0 + R\,\delta\phi + (\delta\phi_C\,\partial R/\partial\phi_C)\,\phi_0, \tag{6}$$

where R is the rate matrix evaluated at the point of maximum wing emission, and the first term on the right side of the equation vanishes, by definition of equilibrium. We can rewrite (6) as

$$\delta\dot{\phi} = [DR]\,\delta\phi, \tag{7}$$

where

$$[DR]_{ij} = [R]_{ij} + \delta_{jC}\,\phi_0 \cdot \partial r_i/\partial\phi_C \tag{8}$$

where δ is the Kroneker delta of rank two and r_i is row i of R.

DR is the desired linearization of the rate matrix in equation (1). It is a 5 by 5 matrix equation, whose size makes its eigenvalues hard to obtain in a simple way. This is further complicated by the fact that there is a very broad spread in the magnitudes of the matrix elements, so that slight errors in the eigenvectors can produce contamination by drastically larger eigenvalues, which makes determination of the actual eigenvalue impossible from knowledge of the approximate normal mode. But since the overall behavior of the system was obtained from the two-level plus continuum model of FCM and it is assumed that inclusion of levels 3 and 4 cannot drastically effect the overall behavior, we looked at the reduced 3 by 3 linearized system and were able to obtain the eigenvalues by simply factoring the characteristic polynomial. This was further aided by the fact that since the rate matrix (and the linearized version) must conserve particle number and therefore must produce time derivatives that add up to zero, it is singular, it has determinent zero, and its range forms a two-dimensional subspace. This singularity results in one of the eigenvalues being zero (corresponding to the non-decaying equilibrium mode itself). Thus finding the remaining eigenvalues amounts to factoring the quadratic polynomial to which the characteristic polynomial reduces.

The results of this simple analysis show that, although the eigenvalues vary over the atmosphere, in the region of greatest wing emission at $\Delta\lambda$ = -1.6 and -1.8 Å we find one dominant eigenvalue of order 10^8 s^{-1}, which is essentially equal to the large 2 → 1 spontaneous decay rate, and a second eigenvalue of size roughly 5 - 10 s^{-1}, which arises from the sum of all the linearized continuum rates except the large 2 → c rate. The corresponding eigenmodes are the direct exchange of electrons between levels 1 and 2, and the exchange of electrons between the continuum and levels 1 and 2 in proportion to the equilibrium ratio between these two levels. It is this second eigenvalue that is related to the ionization timescale, and is believed to account for the equilibration time seen in the blue wing of Figure 2. Since the eigenvalue gives the equilibration rate, its inverse gives the corresponding timescale, which in this case is 0.1 - 0.2 seconds.

This rate appears to be a little too fast to explain the 0.3 - 0.4 s Hα timescale. This could be due to the fact that the linearized rates are high by some factor of order unity owing to the fact that the eventual equilibrium point is not actually within the local range of the validity of the linear approximation until equilibration is nearly attained. Thus during the times of primary interest (0.5 < t < 1.5 s), we are experiencing a drift of the equilibrium point of the local linearization in addition to the linear time evolution toward this point, which extends the equilibration timescale somewhat. This could be enhanced by the nonlocal effects of the radiation field. Since the discrepancy is of order unity, we believe that the ionization process described here does successfully account for, and is the dominant physical effect in, the observed 0.3 - 0.4 s equilibration timescale in the blue wing. Other effects such as changes in the opacity of the optically thin emitting region and variations in the optically thick wing emission from the photosphere due to changes in the total opacity of the chromosphere play a lesser role, and certainly depend on the ionization timescale also.

CHROMOSPHERIC CONDENSATION

Another important timescale that can be inferred from Figure 2 is the timescale for the onset of strong Hα emission from the chromospheric condensation. This is visible as a rapid increase in both line center and red wing emission starting at t ~ 1 s. Shortly thereafter, condensation emission dominates both the red wing and, to a lesser extent, line center. Awareness of this ~1 s delay time is important because this condensation emission could be confused observationally with the initial brightening that occurs when the electron beam is "turned on", particularly in the red wing where the red-shifted condensation emission becomes much stronger than the normal wing emission (which comes from deeper in the chromosphere and produces the initial red wing brightening).

A rough way to see how this ~1 s formation delay time comes about is to imagine a simple two-step model of the effects of the explosive evaporation of the upper chromosphere when the beam is "turned on". In the first step, explosive evaporation causes the pressure to increase very rapidly at the top of the chromosphere. Fisher (1986) has shown that this first step can be understood quantitatively with a simple "gasbag" model of the explosively evaporating region (see Fisher, Canfield and McClymont 1985a). We refer the interested reader to Fisher (1986), and will not discuss this first step further here; we will make the simplifying assumption that this pressure increase is instantaneous (both the FCM simulations and the gasbag model show that it actually takes a few tenths of a second to reach its maximum value). In the second step, the high pressure region moves down into the chromosphere as a compression wave and forms the condensation. This can be modelled most simply as a piston with constant pressure excess Δp behind it moving down into a chromosphere of density ρ, compressing the material ahead of it to the piston pressure. Since we are interested in only ~1 s timescales here, the piston is taken to move at a constant velocity v -- the velocity of the compression wave. Then setting the pressure discontinuity equal to the rate of change of momentum in the compressed material (i.e.,the condensation), we obtain the accretion rate of condensation mass m:

$$\Delta p = \frac{dm}{dt} v = \rho v^2,$$

so that

$$v = \left[\frac{\Delta p}{\rho}\right]^{\frac{1}{2}}.$$

Taking from the simulation a characteristic $\rho \simeq 4\text{x}10^{-12}$ g cm^{-3} and $\Delta p \simeq 200$ dynes cm^{-2} gives $v \simeq 70$ km s^{-1}, comparable to the initial condensation velocity in the $F_{20} = 10^{11}$ ergs cm^{-2} s^{-1} simulation. Then the column accretion rate of hydrogen with a density of roughly 2-3x10^{12} cm^{-3} is about 1-2x10^{19} cm^{-2} s^{-1}. Now from the simulation it is found that the condensation begins to become visible in Hα when it has accumulated a column depth of about 5x10^{18} cm^{-2} and becomes optically thick at about 2x10^{19} cm^{-2}. This simple model thus provides a consistent picture of why it takes about 1 s to begin seeing condensation effects. It should be noted that this delay time will depend on the F_{20} value, and may vary by perhaps a factor of two over a plausible range of explosive F_{20} values.

CONCLUSIONS

We find an Hα response to a instantaneously initiated intense beam of nonthermal electrons that is rapid compared to the timescale associated with the propagation of these electrons over characteristic flare loop dimensions. The amplitude and timescale of this response vary over the Hα profile, and show effects which arise from three different physical mechanisms. First, there is an impulsive initial rise on the chromospheric heating timescale; this rise has greatest amplitude at line center. Second, there is a slower component, on hydrogen ionization timescales, which is most apparent in the blue wing. Third, there is a delayed response associated with the formation of the chromospheric condensation, which is most apparent in the red wing. This latter component dominates over ionization effects on the red side of Hα.

We conclude that observational efforts to detect impulsive Hα brightenings associated with impulsive hard X-ray or microwave bursts should initially focus their attention on line center. Additional simultaneous blue-wing measurements will have diagnostic potential because of their sensitivity to the thermal ionization timescale and the fact that even for very intense electron heating ($F_{20} = 10^{11}$ ergs cm^{-2} s^{-1}) the timescale is in a readily observable range (>0.1 s). However, red wing measurements are potentially deceptive, since the prompt enhancements on the chromospheric heating timescale are much smaller than the ~1 s delayed enhancements due to chromospheric condensations, which are not uniquely associated with either nonthermal electron beams or conduction fronts.

REFERENCES

Brown, J. C., Melrose, D. B., and Spicer, D.S.: 1979, *Astrophys. J.*, 228, 592.

Canfield, R. C., Gunkler, T. A., and Ricchiazzi, P.J.: 1984, *Astrophys. J.*, 282, 296.

Canfield, R. C., McClymont, A. N., and Puetter, R. C..: 1983, in *Methods in Radiative Transfer*, ed. W. Kalkofen (Cambridge: Cambridge University Press), p. 101.

Canfield, R. C. and Ricchiazzi, P. J.: 1981, *Astrophys. J.*, 239, 1036.

Fisher, G. H. 1986, in preparation.

Fisher, G. H., Canfield, R. C. and McClymont, A. N.: 1985a, *Astrophys. J.*, 289, 425.

Fisher, G. H., Canfield, R. C. and McClymont, A. N.: 1985b, *Astrophys. J.*, 289, 434.

Kaempfer, N., and Magun, A.: 1983, *Astrophys. J.*, 274, 910.

Kaempfer, N., and Schoechlin, W.: 1982, *Solar Phys.*, 78, 215.

Lin, R. P., and Hudson, H. S.: 1976, *Solar Phys.*, 50, 153.

Mihalas, D.: 1978, *Stellar Atmospheres* (2nd ed.), W. H. Freeman and Co., San Francisco.

Milkey, R. W., and Mihalas, D.: 1973, *Astrophys. J.*, 185, 709.

Vernazza, J. E., Avrett, E. H., and Loeser, R. 1981: *Astrophys. J. Suppl.*, 45, 619.

Vorpahl, J.: 1972, *Solar Phys.*, 26, 397.

Zirin, H.: 1978, *Solar Phys.*, 58, 95.